Spatiotemporal Dynamics: Applications to vegetation population dynamics

Andreu Fiol Mateu, afiolmat7.alumnes@ub.edu
Facultat de Física, Universitat de Barcelona, Diagonal 645, 08028 Barcelona, Spain.

Advisor (IFISC): Daniel Ruiz-Reynés, druiz@ifisc.uib-csic.es; Tutor (UB):David Reguera, dreguera@ub.edu

Abstract: Vegetation patterns appear in a wide range of ecosystems like drylands, salt marshes or seagrass meadows, forming a large variety of structures like patches of vegetation, fairy circles or vegetation labyrinths. The mechanisms behind the formation of these structures are still a matter of discussion. Our focus is to investigate the origin of a pattern formed by arcs of bare soil in a homogeneous meadow of *Posidonia Oceanica* observed in the Pollença bay (Mallorca). Similar spatial structures emerge from excitable dynamics between vegetation density and sulfide concentration in the soil, like ring-shaped pulses of vegetation propagating through the seabed, as reported by Ruiz-Reynés et al. Here we use bifurcation theory and stability analysis to examine whether these structures could be originated by the same process. The theoretical model used successfully predicts an alternative excitable regime where vegetation transiently disappears before returning to the homogeneous state, which should be compatible with the pattern of arcs mentioned.
Keywords: Dynamical systems, bifurcation theory, pattern formation, theoretical ecology
SDGs: 13. Climate action, 14. Life below water

I. INTRODUCTION

Seagrass meadows are found globally, providing a wide range of ecosystem services that support coastal communities and contribute to environmental health. In the face of climate change and growing pressures on ecosystems, the spatial self-organization of seagrass vegetation has been shown to be a valuable indicator of meadow degradation.
In a favorable environment, vegetation tends to proliferate, forming homogeneous meadows. However, when the mortality rate is high enough, vegetation cannot survive and only bare soil remains. In between these two regimes, scale-dependent feedback becomes dominant, leading to the emergence of spatially heterogeneous vegetation patterns [1, 2].
These inhomogeneities have proven to be useful in identifying the drivers of the spatial organization of vegetation. In this context, heterogeneous patterns have been shown to be a signature of resilience against the deterioration of the environment, helping the meadow cope with challenging conditions by adapting its spatial distribution. Prominent examples of self-organization are arid ecosystems, where the main scale-dependent feedback is the competition for water, which can result in the well known fairy circles found in the Australian desert [3].

Recently, a growing interest has been shown in self-organization of seagrass meadows due to their extensive coverage of the underwater soil as well as their role as critical elements of the marine ecosystems.
In the Mediterranean sea, *Posidonia Oceanica* is considered the most important seagrass species. It provides essential services for the environment such as producing large quantities of oxygen, fixing the values of CO_2, or protecting the soil and the many species that inhabit the area, accumulating large quantities of biomass [4]. Due to it's importance, *Posidonia Oceanica* is commonly used as a marker to determine the state and health of marine ecosystems. However, due to climate change and human activity, it is declining at alarming rates [5].
Posidonia Oceanica can be found in both large homogeneous meadows and heterogeneous patterns like fairy circles observed in the Corsican coast or ring-like pulses of vegetation propagating through bare soil in the Balearic coast (Fig. 1a) [2, 6].

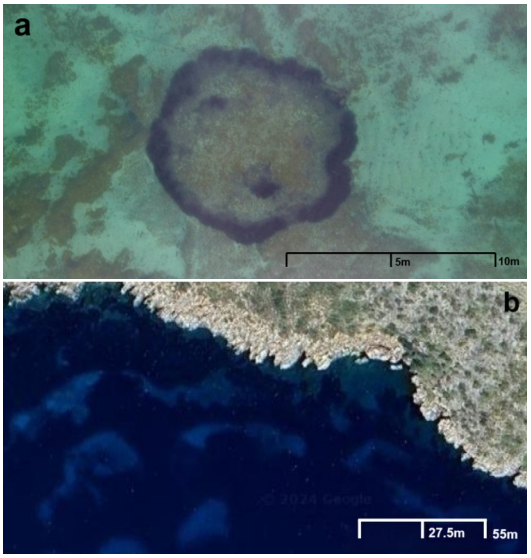

FIG. 1: Spatial structures of *Posidonia Oceanica* seagrass meadows. Panel **a** shows a high resolution image of an excitable ring with an approximate diameter of 10 meters observed in the Pollença bay. Adapted from [7] with permission from the authors. Panel **b** shows arcs of bare soil, approximately 55 meters long, in an homogeneous meadow. Satellite image from Google Maps of the Pollença bay.

A recent study by Ruiz-Reynés et al. has shown that the spatial distribution of these rings can be related to the excitable dynamics resulting from the negative feedback between seagrass growth and sulfide accumulation in the sediment. Hydrogen sulfides are the main byproduct of bacteria in the seagrass sediment. As vegetation proliferates, organic matter is produced, resulting in a higher concentration of sulfides. However, due to their toxicity, sulfides inhibit growth and increase the mortality of the plant, which, in turn, introduces oxygen in the soil to oxidate sulfides as a protection mechanism. Under the right conditions, mathematical modeling predicts the appearance of the excitable rings previously mentioned as a patch of vegetation that starts to decay from it's center as sulfides accumulate. However, at the same time it spreads outward to the surrounding soil, which is less rich in hydrogen sulfide, giving the appearance of an expanding ring [7].
Beyond vegetation rings, other spatial structures have been found underseas, in particular, a pattern of arcs of bare soil embedded in an otherwise homogeneous meadow of seagrass, which can be observed close to the Pollença bay, in Mallorca (Fig. 1b).
In this work it will be shown that the same dynamics linked to the rings of seagrass potentially explain said arcs when considering a larger density-dependent removal rate of sulfides.

II. THEORETICAL MODEL

A model composed of two coupled partial differential equations was used to describe the spatio-temporal evolution of the vegetation density, n, and the sulfide concentration, S [7]:

$$\partial_t n = (\omega_b - \omega_d(n,S))n + d_0\nabla^2 n + d_1(n\nabla^2 n + |\nabla n|^2), \tag{1}$$

$$\partial_t S = c_s\omega_d(n,S)n + P_s - \delta_s S - \delta_0 nS + D_s\nabla^2 S, \tag{2}$$

where ω_b is the branching rate, ω_d is the mortality rate as a function of n and S and d_0 and d_1 describe the spread of clonal plants through space.
Due to organic matter production by the plant, hydrogen sulfide accumulates in the sediment proportionally to dead plants, $\omega_d(n,S)n$, with c_s being the factor determining the increase in concentration per unit of shoot density, P_s represents the external input of sulfides due to the decomposition of organic matter in the soil and $\delta_s + \delta_0 n$ is the removal rate of sulfides, while D_s is the effective diffusion of sulfides.
The mortality rate is described by

$$\omega_d(n,S) = \omega_{d0} - \frac{\omega_{d0}an}{1+an} + bn^2 + \gamma S, \tag{3}$$

where ω_{d0} is the intrinsic mortality rate of the plant, $\frac{\omega_{d0}an}{1+an}$ is a self-saturating term that prompts facilitation: it grows linearly with n until it saturates to the value of ω_{d0} for high density values. bn^2 is a saturation term and γ is the sensibility of the plant to sulfides and measures the increase in mortality rate due to sulfides.
In order to identify the regime suitable for the formation of arcs of bare soil, a stability analysis has been done to determine how the dynamics change with the intrinsic mortality rate, where spatial terms are not considered.

A. Stability analysis and bifurcation theory

The dynamics of vegetation are strongly influenced by the existence of fixed points. Stable points lead to steady solutions with constant density, whereas unstable points cause perturbations to grow.
The fixed points can be found by solving equations $\partial_t n^* = 0$, for which we have $\omega_d(n^*, S^*) = \omega_d^* = \omega_b$, and $\partial_t S^* = 0$ which results in $S^* = \frac{c_s n^* \omega_b + P_s}{\delta_0 n^* + \delta_s}$. Keeping in mind that the bare soil solution, $n^* = 0$, is always a fixed point, independent of the parameters, the other fixed points are given by:

$$\omega_{d0} = \left(\omega_b - b{n^*}^2 - \gamma\frac{c_s\omega_b n^* + P_s}{\delta_0 n^* + \delta_s}\right)(1+an^*). \tag{4}$$

From the solution of Eq. 4 the bifurcation diagram can be plotted parametrizing n^* in $\omega_{d0}(n^*)$ as shown in Fig. 2b, where the different regimes are more distinguishable.

The stability of the fixed points can be determined by analyzing the linearized system [8, 9]. We linearize around the fixed points considering a perturbation of the type $n = n^* + \delta n$ and $S = S^* + \delta S$, doing a first order approximation around the fixed point we get the linear system:

$$\begin{aligned}\partial_t \delta n &= (\omega_b - \omega_d^* + \frac{\omega_{d0}an^*}{(1+an^*)^2} - 2b{n^*}^2)\delta n - \gamma n^*\delta S,\\ \partial_t \delta S &= [c_s(\omega_d^* + 2bn^* - \frac{\omega_{d0}an^*}{(1+an^*)^2}) - \delta_0 S^*]\delta n + \\ &\quad + (c_s\gamma n^* - \delta_s - \delta_0 n^*)\delta S,\end{aligned} \tag{5}$$

which can be diagonalized to find the eigenvalues of the system. For $n^* = 0$ we find that the eigenvalues are $\lambda_+ = \omega_b - \omega_{d0} - \frac{\gamma P_s}{\delta_s}$ and $\lambda_- = -\delta_s$, so the unpopulated solution is an unstable point for $\omega_{d0} < \omega_d - \frac{\gamma P_s}{\delta_s}$ as one of the eigenvalues is positive, whereas it is a stable point otherwise (both eigenvalues become negative).

The eigenvalues for $n^* \neq 0$ have been solved numerically due to the complexity of the expression, being a function of all nine parameters. We depict the phase diagram in Fig. 2, while the dependence of the eigenvalues can be seen in the Supplementary Material A.

From the stability analysis, three types of bifurcation points (thresholds where the system changes its behaviour) have been identified.
A saddle point marks the disappearance of two merging fixed points and it can be found where one of the eigenvalues becomes zero. However, in this case it was determined by finding the roots of the derivative of Eq. (4) respect to n^*. In a transcritical bifurcation two fixed points collide and change stability. Although one of the eigenvalues also becomes zero, in this work it is found by imposing $n^* = 0$ to Eq. (4), resulting in $\omega_{d0} = \omega_b - \gamma \frac{P_s}{\delta_s}$. Notice that this bifurcation marks the change in stability of the bare soil solution. A Hopf bifurcation can be found in regimes where the eigenvalues are complex conjugates, resulting in a system that evolves in a spiral around the fixed point. If the real part of the eigenvalues is negative, the spiral converges into the fixed stable point. However, if the real part of the eigenvalues is positive, perturbations grow over time, eventually reaching a limit cycle, so the fixed point becomes unstable. The transition between these two regimes is known as a Hopf bifurcation, marking the onset of an oscillatory regime [8].

III. RESULTS AND DISCUSSION

For a better understanding of the model and how excitability emerges from its dynamics, we will first present the results we obtained with the realistic parameters used to model the excitable rings [7]:
As Fig. 2 shows, for a low mortality rate and low sensitivity to sulfides the model predicts a single high-density stable point and an unstable point for $n^* = 0$. This means that vegetation will easily appear and evolve quickly towards the stable point, where it will form an homogeneous meadow (Fig. 3a). In contrast, for high values of mortality and sensitivity, plants cannot grow and $n^* = 0$ becomes the only stable point, resulting in bare soil as the only possible outcome. For intermediate values of mortality and sensitivity a Hopf bifurcation appears and the fixed point becomes unstable as a limit cycle gains stability (Fig. 3b). This would result in an oscillatory regime driven by the negative feedback between sulfides and vegetation: density grows increasing sulfide concentration until it is high enough that the mortality rate becomes larger than the branching rate, leading to vegetation decline. Then, sulfides dissipate until the sulfide concentration is low enough for vegetation to grow again and repeat the cycle. Between the transcritical bifurcation and the saddle node bifurcation, for intermediate mortality and low sensitivity, facilitation allows for a bistable regime, introducing a threshold for density to grow defined by an unstable branch of fixed points (Fig. 2). Vegetation below the unstable branch will not have enough strength to grow and will die quickly. However, given an initial condition above the unstable branch, vegetation will grow to reach the stable point (low sensitivity) or the limit cycle (intermediate sensitivity).
In the region where oscillations and bistability overlap, and only if the stable orbit of the oscillatory regime crosses the unstable branch, the cycle is destroyed and the dynamics become excitable, as shown in Fig. 2b. In

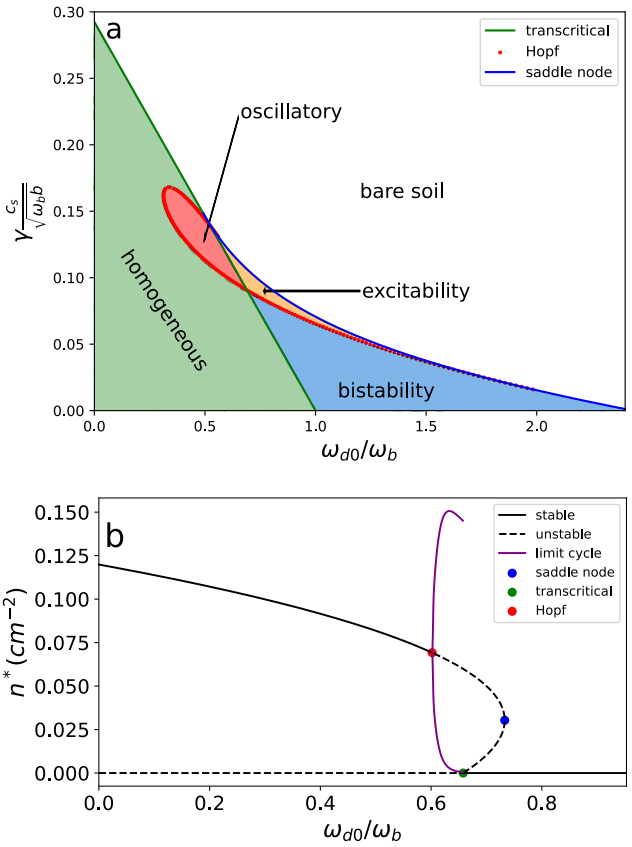

FIG. 2: Different regimes predicted by the model. Panel **a** shows the phase diagram of the system with mortality, ω_{d0}, and sensitivity to sulfides, γ, (dimensionless) as control parameters. The green line represents the transcritical bifurcation, the Hopf bifurcations are represented by the red line and the saddle node bifurcations by the blue line. In the green shaded area, the only steady solution is an homogeneous meadow of vegetation. The red shaded area marks the oscillatory regime. For large mortality but low sensitivity, in the blue area, there are two stable solutions: the homogeneous meadow and the bare soil solution. In the white area vegetation can not grow due to the large mortality and sensitivity to sulfides, so bare soil is the only stable solution. The yellow area marks the excitable regime. Panel **b** shows the bifurcation diagram for $\gamma \frac{c_s}{\sqrt{\omega_b b}} = 0.1$, where the fixed points of the system (stationary values of vegetation density, n^*) as a function of mortality rate, ω_{d0} are represented. The solid line accounts for the stable points whilst the dotted line represents the unstable points, the purple line shows the maximum and the minimum of the limit cycle and the colored dots mark the different types of bifurcations identified.

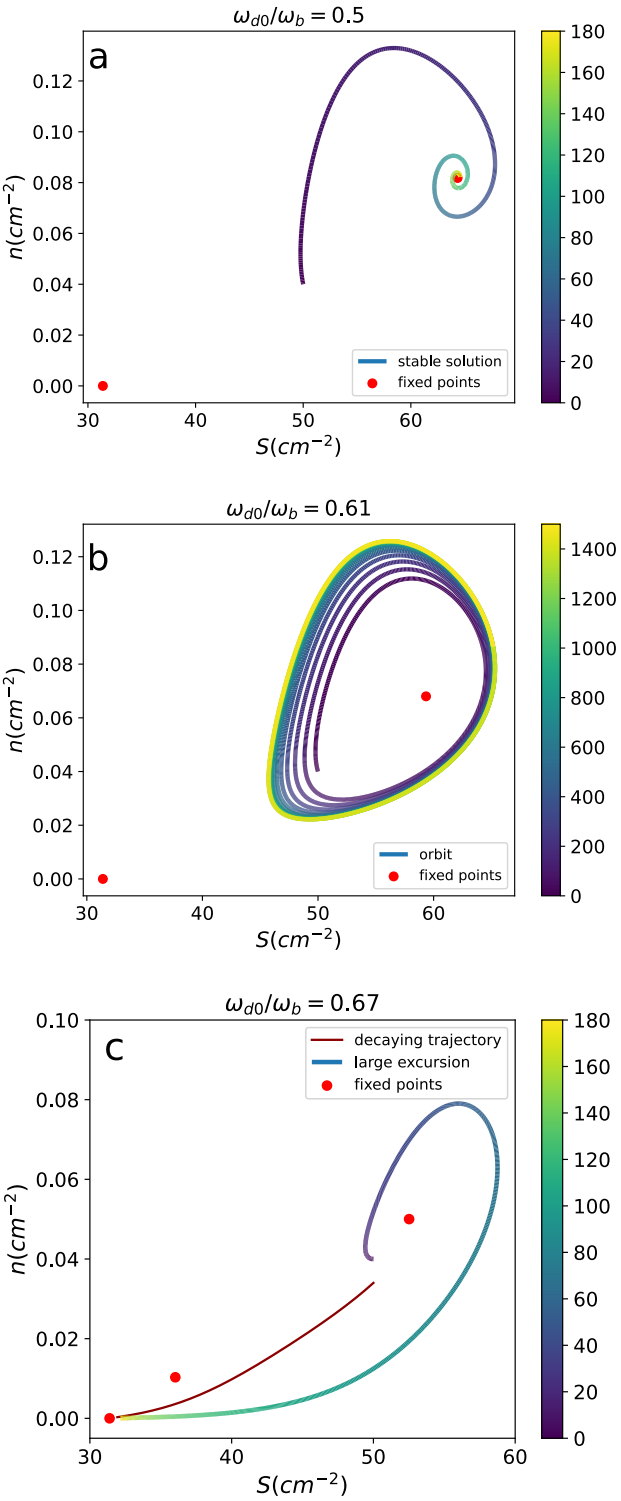

FIG. 3: Evolution of the system for different values of ω_{d0} with the same initial conditions. We plotted the vegetation density, n, as a function of the sulfide concentration, S, with a colored line representing the time scale in years. Panel **a** shows an homogeneous regime: the systems evolves in a quick inward spiral towards the stable point. Panel **b** shows an oscillatory regime: the system stabilizes in an orbit around the now unstable point. Finally, panel **c** shows an excitable regime, comparing the decaying trajectory with the large excursion trajectory.

this case, given an initial condition above the threshold, the system grows mirroring the destroyed limit cycle, hoping to reach the stable orbit. However, sulfides do not fade fast enough, so the system crosses the unstable branch and decays inevitably to zero (Fig. 3c).

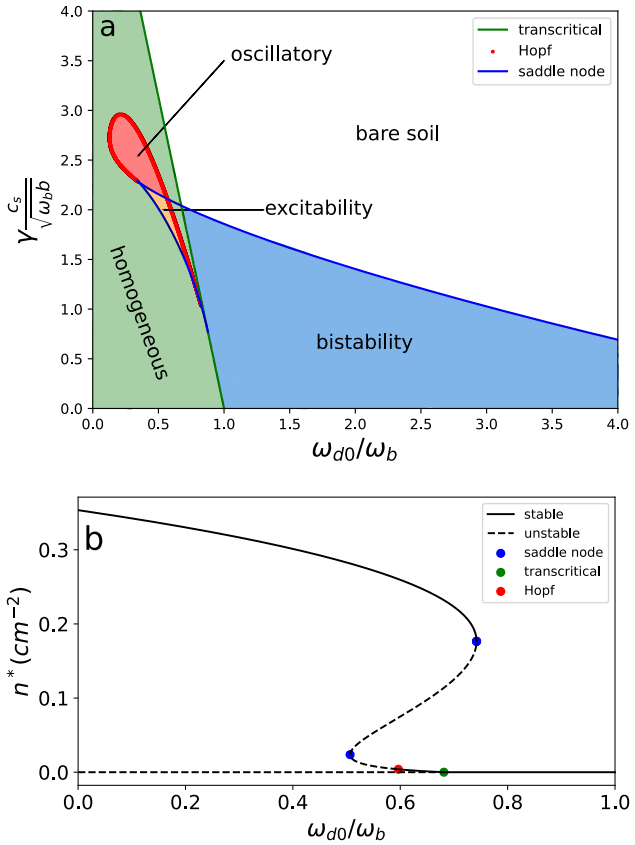

FIG. 4: Different regimes predicted by the model for the new-found parameters. Panel **a** shows the phase diagram of the system. A second saddle node appears which merges with the transcritical bifurcation as sensitivity decreases. The excitable regime is now before the transcritical bifurcation, between the new saddle node bifurcation and the Hopf bifurcation. The parameters used are: $\omega_b = 1.0$ y^{-1}, $a = 19.0$ cm^2, $b = 1.67$ cm^{4}y^{-1}, $c_s = 90$ μMcm^2, $P_s = 0.4$ μMy^{-1}, $\delta_s = 0.036$ y^{-1}, $\delta_0 = 3.2$ cm^{2}y^{-1}, $\gamma = 6.54 \cdot 10^{-3}$ μM^{-1}y^{-1}. Panel **b** shows the bifurcation diagram for $\gamma \frac{c_s}{\sqrt{\omega_b b}} = 2.0$.

When the removal rate of sulfides due to vegetation, δ_0, is largely augmented (in this project it was increased from 0.06 cm^{2}y^{-1} to 3.2 cm^{2}y^{-1}) the bifurcation diagram shows multiple folds for $\gamma \frac{c_s}{\sqrt{\omega_b b}} \in [1.0, 2.1]$. As a result, a second saddle node appears and the Hopf bifurcation moves to the lower branch of stable points, with an oscillatory regime between them for low densities of vegetation (Fig. 4). This region gathers all requirements for excitability to emerge due to the destruction of the limit cycle when it crosses the unstable branch, allowing vegetation to grow to the high-density solution (Fig. 5). In this regime, a low-density meadow would decay to

bare soil due to the high concentration of sulfides, which we hypothesize would form the arc structures shown in Fig. 1 if a spatially extended system was considered. However, as a result of the now faster removal rate of sulfides, vegetation would grow again where mortality was too high for vegetation to proliferate before, forming the high-density homogeneous meadow that surrounds the structures. It is also noticeable that the high removal rate of sulfides allows vegetation to achieve stability at a much higher density compared to the previous set of parameters. Moreover, a stable solution corresponding to a low-density homogeneous meadow is found between the Hopf bifurcation and the transcritical bifurcation for initial conditions below the unstable branch (Fig. 4b).

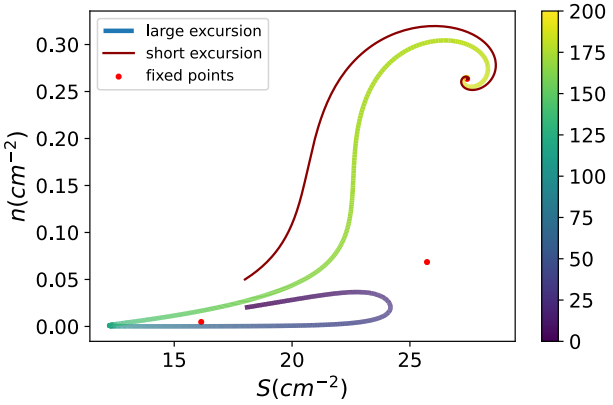

FIG. 5: Evolution of the system in the new excitable regime with $\omega_{d0}/\omega_b = 0.585$. The coloured line represents the evolution in years followed in the excitable regime, with initial conditions below the threshold ($n_0 = 0.02$ cm^{-2} and $S_0 = 18$ cm^{-2}), in brown the evolution of the system with initial conditions above the unstable branch ($n_0 = 0.05$ cm^{-2} and $S_0 = 18$ cm^{-2}). The red dots mark the fixed points.

IV. CONCLUSIONS

The theoretical results obtained in this project successfully reproduce the results obtained by Ruiz-Reynés et al., using linear stability analysis to associate the excitable dynamics that emerge from the mathematical model with the ring-like pulses observed in the Pollença bay. Furthermore, new parameter regimes have been identified that potentially support the arcs of bare soil observed in the Mediterranean sea, establishing a connection between these structures and a larger density-dependent removal rate of sulfides. For further proof of the compatibility with this pattern, spatio-temporal simulations are required, which we intend to do in the near future.

As other structures, the formation of these arches could be a method of resilience against harsh conditions in the environment, adapting the spatial distribution to higher mortalities in order to survive. Excitability in this system allows low-density meadows to thrive and reach high-density stability in a region that otherwise would be restricted to a low-density oscillatory regime. Hence the importance of tracking these structures and understanding the mechanisms that drive them, as they are key factors in assessing the ecosystems health conditions.

Acknowledgments

I would like to thank my advisors from IFISC, Dr. Damià Gomila and, specially, Dr. Daniel Ruiz-Reynés, for their trust and guidance through all this work and having the confidence in me to let me participate in this amazing project. I would also like to thank Dr. David Reguera, my tutor from the University of Barcelona, for his genuine interest in the project and ensuring it was successful. I would also like to thank the IFSIC institution for the opportunity to work in this project as well as the physics department's adiministration of the UB for facilitating the agreement between both institutions, making this thesis possible.

[1] Rietkerk, M. et al. "Evasion of tipping in complex systems through spatial pattern formation". Science **374**:eabj0359 (2021).
[2] Ruiz-Reynés, D. et al. "Fairy circle landscapes under the sea". Sci. Adv. **3**: e1603262 (2017).
[3] Getzin, S. et al. "Discovery of fairy circles in Australia supports self-organization theory". Proc. Natl. Acad. Sci. U.S.A. **113**: 3551-3556 (2016).
[4] Barbier, E. et al. "The value of estuariane and coastal ecosystem services". Ecologycal Monographs, **81**:169-193
[5] Marbà, N. et al. "Mediterranean seagrass (Posidonia oceanica) loss between 1842 and 2009". Biological Conservation **176**: 183-190 (2014)
[6] Pasqualini, V. et al. "Environmental impact identification along the Corsican coast (Mediterranean sea) using image processing". Aquatic Botany **65**: 311-320 (1999).
[7] Ruiz-Reynés, D. et al. "Self-organized sulfide-driven traveling pulses shape seagrass meadows". Proc. Natl. Acad. Sci. U.S.A. **120**: e2216024120 (2023).
[8] Steven H. Strogatz, *Nonlinear Dynamics and Chaos: With Applications to Physics, Biology, Chemistry, and Engineering*, (Westview Press, Cambridge, MA, 1994, 1st. ed.).
[9] Meron, E. "Pattern formation in excitable media". Physics Reports **218**: 1-66 (1992)

Dinàmica espaciotemporal: Aplicacions a la dinàmica de població de la vegetació

Andreu Fiol Mateu, afiolmat7.alumnes@ub.edu
Facultat de Física, Universitat de Barcelona, Diagonal 645, 08028 Barcelona, Spain.

Advisor (IFISC): Daniel Ruiz-Reynés, druiz@ifisc.uib-csic.es; Tutor (UB):David Reguera, dreguera@ub.edu

Resum: En una gran varietat d'ecosistemes s'ha observat que la vegetació pot formar una àmplia gamma de patrons heterogenis, com els anomenats cercles de fades observats tant en regions àrides com en praderes de plantes marines, laberints de vegetació, o regions on les plantes creixen formant flocs aïllats. En aquest treball s'investiga l'origen d'unes estructures en forma d'arcs sense vegetació a l'interior d'una pradera de *Posidònia Oceànica* observades a la badia de Pollença, a Mallorca. Recentment s'ha determinat que estructures similars emergeixen de la dinàmica excitable entre la vegetació i la concentració de sulfur d'hidrogen al sòl marí, com és el cas d'uns polsos de vegetació en forma d'anell que es propaguen pel sòl en la mateixa badia de Pollença. Mitjançant teoria de bifurcacions i anàlisi d'estabilitat s'estudia si el mateix procés podria resultar en aquestes estructures en forma d'arc. El model teòric emprat prediu amb èxit un règim excitable en el qual la vegetació desapareix durant un cert temps abans de tornar a créixer fins estabilitzar-se en un estat homogèni, potencialment compatible amb els arcs mencionats.
Paraules clau: Sistemes dinàmics, bifurcacions, resolució numèrica
ODSs: Aquest TFG està relacionat amb els Objectius de Desenvolupament Sostenible (SDGs) 13. Acció climàtica, 14. Vida submarina

Objectius de Desenvolupament Sostenible (ODSs o SDGs)

1. Fi de les desigualtats	10. Reducció de les desigualtats	
2. Fam zero	11. Ciutats i comunitats sostenibles	
3. Salut i benestar	12. Consum i producció responsables	
4. Educació de qualitat	13. Acció climàtica	X
5. Igualtat de gènere	14. Vida submarina	X
6. Aigua neta i sanejament	15. Vida terrestre	
7. Energia neta i sostenible	16. Pau, justícia i institucions sòlides	
8. Treball digne i creixement econòmic	17. Aliança pels objectius	
9. Indústria, innovació, infraestructures		

El contingut d'aquest TFG, part d'un grau universitari de Física, es relaciona amb l'ODS 13, i en particular amb la fita 13.1, ja que estudia els mecanismes que governen la dinàmica de la vegetació, coneixement essencial a l'hora d'evaluar la salut dels ecosistemes i potencials factors de risc. Aquest coneixement permetrà buscar solucions davant la pressió que el canvi climàtic exerceix sobre el medi ambient. Pel mateix motiu també es pot relacionar amb l'ODS 14, fites 14.2 i 14.a, ja que s'estudien estructures de posidònia, una de les espècies de planta submarina més importants pels ecosistemes del Mediterrani.

GRAPHICAL ABSTRACT

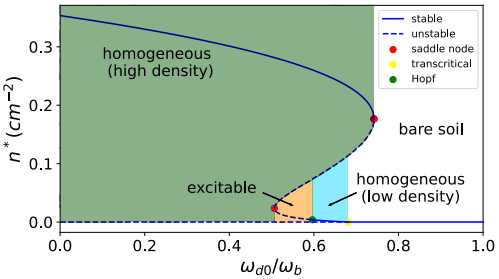

FIG. 6: Bifurcation diagram using a set of parameters compatible with the arcs of bare soil

SUPPLEMENTARY MATERIAL

A. Analysis of the eigenvalues of the system

As additional information, the eigenvalues of the populated solution as functions of the mortality rate are shown in this section to further discuss the lineal analysis and the determination of the bifurcation points.
The eigenvalues for the populated solution can be found solving the second order expression $\lambda^2 + B\lambda + C = 0$, where

$$B = -(c_s\gamma n^* - \delta_s - \delta_0 n^* + \frac{\omega_{d0} a n^*}{(1+an^*)^2} - 2bn^{*2}),$$
$$C = \omega_b c_s \gamma n^* - \delta_0 S^* \gamma n^* - \left(\frac{\omega_{d0} a n^*}{(1+an^*)^2} - 2bn^{*2}\right)(\delta_s + \delta_0 n^*),$$

and we have previously solved Eq. 4 numerically to find $n^*(\omega_{d0})$.
The numerical solution obtained for the eigenvalues belonging to the fixed points obtained with the realistic parameters used to describe the excitable rings can be seen in Fig. 7.

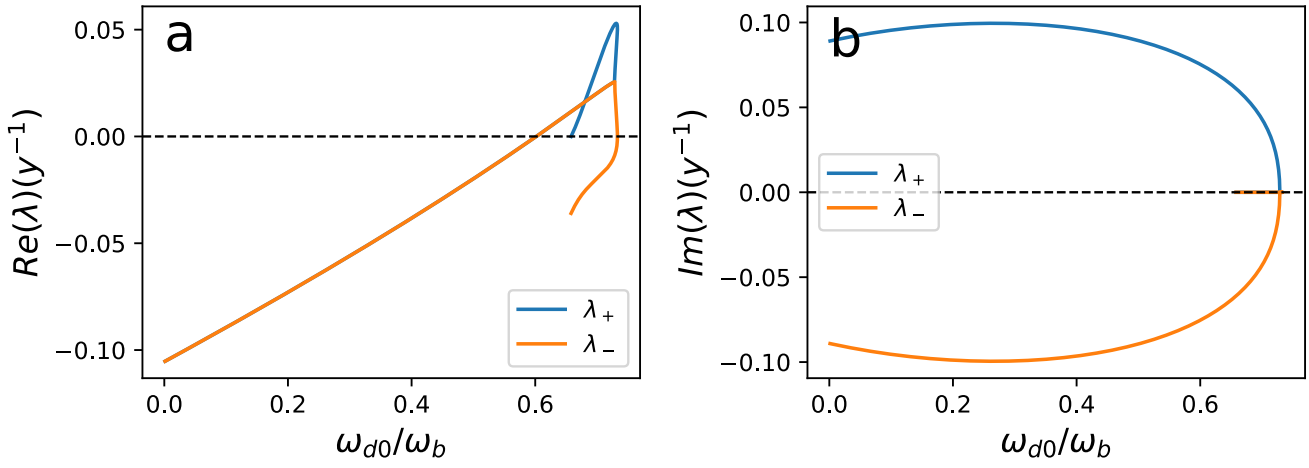

FIG. 7: Eigenvalues belonging to the fixed points of the populated solution with realistic parameters corresponding to excitable rings. Panel **a** shows the real part of the eigenvalues while panel **b** shows the imaginary part.

Comparing Fig. 2b and Fig. 7, it is noticeable that while the fixed points are stable, with a low mortality rate, the eigenvalues are complex conjugates with a negative real part, hence the spiral evolution of the system towards the stable point (Fig. 3a). As expected, the Hopf bifurcation is found where the real part of the eigenvalues becomes zero, and in the oscillatory regime the eigenvalues are still complex conjugates, but with a positive real part. At the end of the oscillatory regime both eigenvalues become real as the imaginary part vanishes. Furthermore, both the transcritical bifurcation and the saddle node bifurcation align with one of the eigenvalues becoming zero, and in the lower branch the eigenvalues have opposite sign, making it unstable.

For the parameters in which we found the excitable regime associated with the arcs of bare soil, the numerical solution of the eigenvalues can be seen in Fig. 8.

Comparing with Fig. 4b, eigenvalues for the low mortality, high-density solution are also complex conjugates with a negative real part, so the system would evolve in a convergent spiral similar to Fig. 3a toward the stable fixed point. Then both eigenvalues become real and, after the saddle node bifurcation, one becomes positive, resulting in the unstable branch, which ends in a second saddle node bifurcation. In the last section, the eigenvalues become complex conjugates again, with an oscillatory regime (positive real part) for low mortality rate, and a short stable region after the Hopf bifurcation (negative real part).

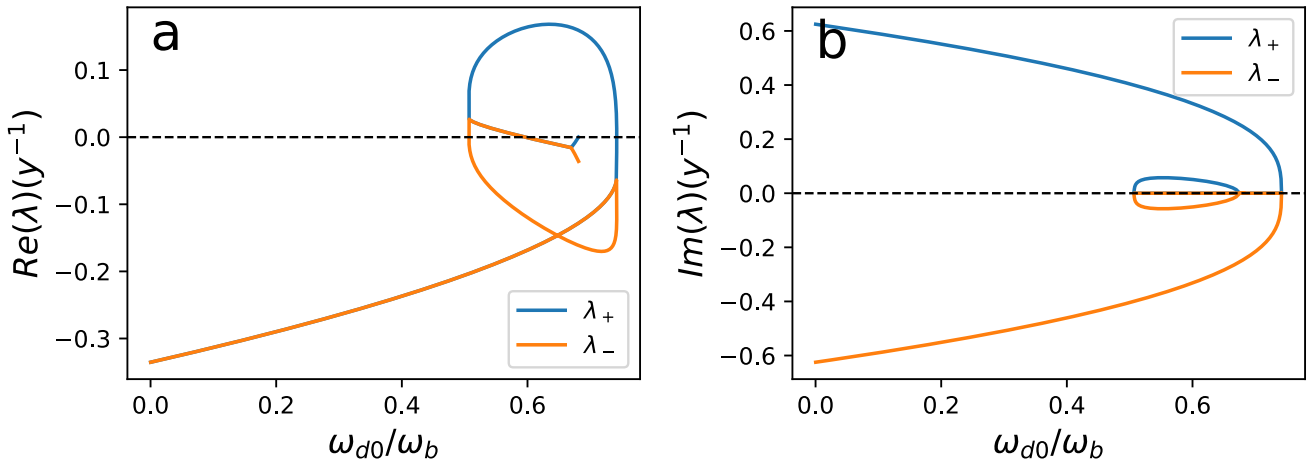

FIG. 8: Eigenvalues belonging to the fixed points of the populated solution with the parameters corresponding to excitable arcs. Panel **a** shows the real part of the eigenvalues while panel **b** shows the imaginary part.

B. Numerical methods

To find the fixed points and bifurcations, the corresponding equations have been solved numerically using methods like bisection or Newton-Raphson, using Fortran90 as the programming language.
To compute the evolution of the system, a Runge-Kutta4 method was used to solve the coupled differential equations (1) and (2) (without spatial terms). A step of between $h = 0.1$ year and $h = 1$ year has been used, depending on the precision needed for the concrete regime. The initial conditions have been chosen based on streamline diagrams and the bifurcation diagrams obtained.